Journal of Materials Chemistry A

RSC Publishing

PAPER

View Article Online
View Journal | View Issue

Cite this: J. Mater. Chem. A, 2013, 1, 6004

Overcoming interface losses in organic solar cells by applying low temperature, solution processed aluminum-doped zinc oxide electron extraction layers†

Tobias Stubhan,*[a] Ivan Litzov,[a] Ning Li,[a] Michael Salinas,[b] Matthias Steidl,[a] Gerhard Sauer,[a] Karen Forberich,[a] Gebhard J. Matt,[a] Marcus Halik[b] and Christoph J. Brabec[ac]

Intrinsic zinc oxide (ZnO) is widely used as an electron extraction layer (EEL) for inverted polymer solar cells. Despite the excellent device performance, a major drawback for large area production is its low conductivity. Using microscopic simulations, we derived a technically reasonable threshold value of 10^{-3} S cm^{-1} for the conductivity required to overcome transport limitations. For conductivity values typical for ZnO we observed the interface layer thickness restriction at only a few tens of nanometers, either as a fill factor drop due to serial resistance, eventually accompanied by a second diode behavior, or by the need for light soaking. Higher conductive aluminum-doped zinc oxide (AZO), which was introduced earlier, meets the desired conductivity threshold, however, at the cost of high temperature processing. High annealing temperatures (>150 °C) significantly improve the electrical properties of ZnO, but prohibit processing on plastic substrates or organic active layers. Here we report on AZO layers from a sol–gel precursor, which has been already reported to give sufficiently high conductivities at lower processing temperatures (<150 °C). We investigate the influence of different precursor compositions on the electrical properties of the thin films and their performance in inverted poly(3-hexylthiophene):[6,6]-phenyl-C_{61}-butyric acid methyl ester (P3HT:PCBM) solar cells. Low temperature AZO layers with thicknesses up to 680 nm maintained comparable performance to devices with thin AZO layers.

Received 11th March 2013
Accepted 14th March 2013

DOI: 10.1039/c3ta10987a

www.rsc.org/MaterialsA

1 Introduction

After fast progress in increasing efficiency of organic solar cells, the important 10% hurdle has been overcome,[1–3] and even higher efficiencies of up to 15% are becoming realistic by exploring tandem technologies. Nevertheless, further tremendous efforts are required to develop the OPV technology towards industrial standards. One of the essential, remaining problems is to develop reliable and environmentally stable as well as mechanically robust interfaces. Today's high performance polymers, with only a few exceptions, only perform well in the thin film limit around 100 nm (ref. 4) and frequently suffer from a fill factor reduction upon increased film thickness. Either mobility limitations or a poor morphology in the thick film limit are the reasons for that.[5,6] However, such thin active layers bear the risk of thin film defects, like *e.g.* shunts, negatively impacting yield and reliability of the production process.[6] A straightforward approach would be to develop polymers that also perform well in thick layers.[6] This is not only challenging from the chemical side, but also unwanted from the economical point of view, since thicker films require more of the rather expensive polymers. Other solutions need to be developed, since material expenses dominate the balance of modules (BOM) for fast and large scale printing processes.

An alternative but smart solution is the reengineering of the electrodes and electrode interface layers such that they provide the necessary reliability for the layer stack. Thick, stable and robust interface layers, deposited at low temperatures, "encapsulating" thin active layers is a viable route to achieve this. Considering the material properties of known interface layers, poly(3,4-ethylene dioxythiophene):(polystyrene sulfonic acid) (PEDOT:PSS) as the p-type side extraction layer meets most requirements. PEDOT:PSS has a widely tunable conductivity and is processed at low temperatures. The drawbacks of PEDOT:PSS are stability concerns, mainly due to the

[a]Institute of Materials for Electronics and Energy Technology (I-MEET), Friedrich-Alexander-University Erlangen-Nuremberg, Martensstrasse 7, 91058 Erlangen, Germany. E-mail: tobias.stubhan@ww.uni-erlangen.de; Fax: +49-(0)9131/85-28495; Tel: +49-(0)9131/85-27634

[b]Organic Materials and Devices (OMD), Institute of Polymer Materials, Friedrich-Alexander-University Erlangen-Nuremberg, Martensstraße 7, 91058 Erlangen, Germany

[c]Bavarian Center for Applied Energy Research (ZAE Bayern), Haberstr. 2a, 91058 Erlangen, Germany

† Electronic supplementary information (ESI) available. See DOI: 10.1039/c3ta10987a

hygroscopic and acidic nature.[7–9] More stable alternatives for PEDOT:PSS are currently being investigated. In the main focus are transition metal oxides like WO_3,[10] MoO_3,[11] V_2O_5 (ref. 12) and NiO.[13] This material class is still under development, mainly solving solution processing issues. Low conductive, intrinsic layers of these materials can be processed up to around 50 nm thickness without limiting device performance.[10–12] Therefore PEDOT:PSS is still an attractive choice for thick and robust p-type interfaces in the regime of 100 nm and above.

In this report, we focus on the n-type side. The commonly employed EEL materials are TiO_x (ref. 14 and 15) and ZnO.[14,16–19] The problem setting is similar to the p-type side. Intrinsic ZnO and TiO_x show low conductivities and therefore are limited in the layer thickness. Recent reports showed that using doped metal oxides with enhanced conductivity is a viable path to overcome this restriction.[20,21] ZnO is a prototype material system for doping investigations. Puetz *et al.* used an indium-doped ZnO nanoparticle solution to process EELs with up to 160 nm thickness without great impact on series resistance (R_S) and fill factor (FF).[21] In recent reports from our group we demonstrated the benefits of aluminum-doped zinc oxide (AZO) layers over intrinsic zinc oxide when using thick films over 100 nm.[20] The disadvantage of this AZO, which was processed from a zinc acetate-based precursor with an aluminum acetate (AlAc) dopant, was the quite high processing temperature of 260 °C for the calcination of the film. Annealing of this AZO formulation at temperatures below 150 °C did not lead to significant conductivity enhancement as compared to intrinsic zinc oxide. Heating to 260 °C increased the conductivity of this AZO precursor by three orders of magnitude ($\sim 10^{-3}$ S cm^{-1}) compared to intrinsic ZnO films ($\sim 10^{-6}$ S cm^{-1}).[20]

Typically OPV processing requires temperatures below 150 °C. To achieve this, we systematically varied the composition of the AZO precursor formulations and investigated its influence on the thin film electrical properties.[22] The best performance was found for AZO layers with an aluminum nitrate (AlNi) dopant, and a conductivity of 7×10^{-3} S cm^{-1} at 140 °C was found. This is comparable to the previously investigated films with an AlAc dopant, when treated at 260 °C (4×10^{-3} S cm^{-1}).[20] As expected, solar cell results confirm these two EEL layer materials as comparable. Numerical simulations further confirm that a conductivity of $>10^{-3}$ S cm^{-1} is required to extend the EEL layer thickness beyond 100 nm. Finally, AZO EELs with over 600 nm film thickness were integrated in P3HT:PCBM solar cells which still showed high efficiency and low series resistance.

2 Results and discussion

2.1 Simulation

We simulated the electrical behavior of the devices by solving the 1d microscopic transport equations with the software PC1D.[23] Fig. 1 shows the experimentally investigated device stack as well as the simplified stack used for the microscopic simulation. The thickness and the conductivity (σ) of the interface layer were systematically varied over a wide range of parameters. The parameter set used for the simulation is given

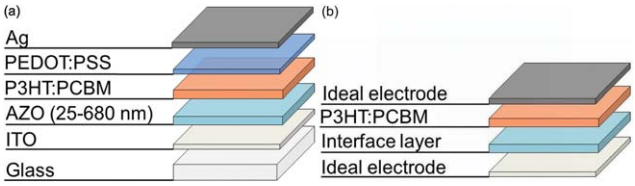

Fig. 1 (a) Layer stack of investigated devices and (b) simplified stack for electrical simulations.

in ESI S1.† Fig. 2 shows the results for conductivities of 1×10^{-3} and 1×10^{-4} S cm^{-1} with a variation of thicknesses ranging from 30 to 1250 and 30 to 750 nm, respectively. For a conductivity of 1×10^{-3} S cm^{-1}, no limitation due to the increased interface layer thickness is observed from the device performance. In contrast, a conductivity of only 1×10^{-4} S cm^{-1} is clearly limiting the device performance due to an increased series resistance for thicker films. If the conductivity is further reduced, the typical s-shape behavior in the *j–V* characteristics is found (see ESI S2†).[24] In conclusion, numerical simulations suggest that a conductivity of $\geq 1 \times 10^{-3}$ S cm^{-1} for the interface layer is sufficient to process thick (*i.e.* >100 nm) electron extraction layers. These simulations did not take into account secondary effects like contact barriers, photoconductivity, shunts or photoshunts as well as microstructure changes in the thick film limit (interface and/or active layer).

2.2 Characterization of AZO layers from different precursor formulations

Three different precursor formulations based on zinc acetate were synthesized to determine the relationship between the composition and film properties (Fig. 3). Either aluminum acetate (AlAc) or aluminum nitrate (AlNi) was used as a dopant. Apart from that the precursor formulations were stabilized with ethanolamine (MEA) or filtered after reaction. The three investigated formulations were (i) AZO 1 (AlAc dopant, MEA stabilized), (ii) AZO 2 (AlAc dopant, no stabilization, filtered) and (iii) AZO 3 (AlNi dopant, no stabilization, filtered).

The resulting conductivities of the films were measured in the 2 point probe geometry as a function of two different annealing temperatures: 140 °C or 260 °C (see Table 1). 140 °C is a suitable temperature for plastic substrates and for the deposition onto organic films, while 260 °C is chosen as a reference.[20] As reported before, AZO 1 reaches a conductivity value in the order of 10^{-3} S cm^{-1} after annealing at 260 °C, while annealing at lower temperatures results in conductivities in the order of 10^{-5} S cm^{-1}. AZO 2 shows a conductivity of 10^{-4} S cm^{-1} at 140 °C, which is already close to the target conductivity. The best conductivity at 140 °C annealing is found for AZO 3 with 7×10^{-3} S cm^{-1}. AZO 3 at 140 °C has conductivity similar to AZO 1 at 260 °C.

Interestingly, AZO 2 and 3 show even higher conductivities above 10^{-1} S cm^{-1} when annealed at 260 °C. A possible explanation for this improvement, when the precursor solution is filtered instead of stabilized, is that MEA forms metal–organic complexes with zinc acetate.[25,26] These complexes need higher

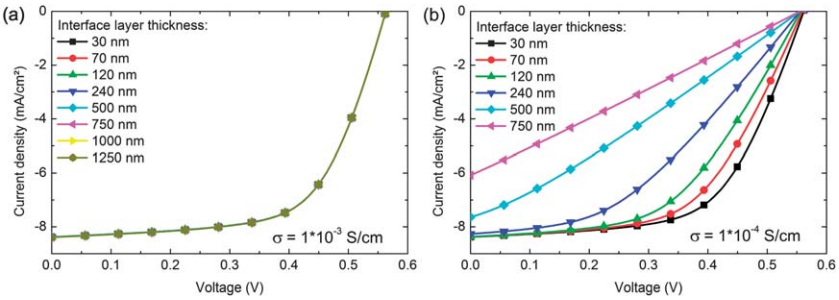

Fig. 2 Simulated *j–V* characteristics with varying interface layer thicknesses for a conductivity of 1×10^{-3} (a) and 1×10^{-4} S cm^{-1} (b). No limitation of device performance is observed for 1×10^{-3} S cm^{-1}, while 1×10^{-4} S cm^{-1} heavily reduces the device performance with increasing interface layer thickness.

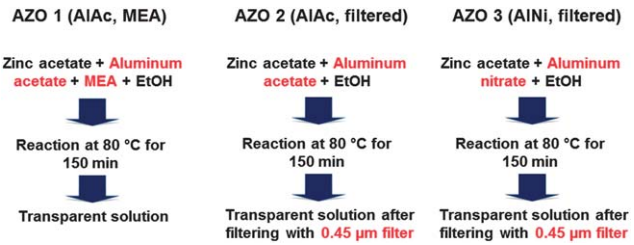

Fig. 3 Schemes of the synthesis routes for the three investigated AZO precursor formulations.

Table 1 Comparison of conductivity values for layers from different precursors as a function of annealing temperatures: 140 °C or 260 °C. The samples were annealed in air. The conductivity was measured in a glovebox (N_2)

	Conductivities (S cm^{-1})	
Materials	140 °C	260 °C
AZO 1 (AlAc, MEA)	8×10^{-5}	$\mathbf{4 \times 10^{-3}}$
AZO 2 (AlAc, filtered)	3×10^{-4}	7×10^{0}
AZO 3 (AlNi, filtered)	$\mathbf{7 \times 10^{-3}}$	6×10^{-1}

temperatures to decompose. The benefit of exchanging AlAc by AlNi is most likely due to the better solubility of AlNi in ethanol. This could promote a more homogenous distribution of Al in the precursor complex and result in a more effective doping. To investigate the nature of the observed conductivity variations, the mobility (μ_{FET}) of the AZO 1 and 3, annealed at either 140 °C or 260 °C, was measured in the thin film transistor geometry. All films showed a μ_{FET} in the range of 0.5–5.3 $\times 10^{-3}$ cm^2 V^{-1} s^{-1} (see ESI S3†). As the conductivity ($\sigma = en\mu$; e = elementary charge, n = carrier concentration, μ = mobility) of the four films varies by 4 orders of magnitude, the major influence on the conductivity is assigned to an increase in the carrier concentrations rather than in the mobility.

According to the conductivity investigations, LT AZO (AZO 3 at 140 °C) was chosen for solar cell testing and referenced to the previously reported HT AZO (AZO 1 at 260 °C). The work function of LT AZO was measured using a Kelvin probe to −4.4 eV. This is sufficiently low to properly contact the lowest unoccupied molecular orbital (LUMO) of PCBM (at −4.3 eV) and is further comparable to the previously reported −4.2 eV for HT AZO.[20] The LT AZO layers have a high transmission, comparable to the previously investigated (doped) zinc oxides (see ESI S5†). The optical bandgap was calculated from a Tauc-plot to 3.3 eV, assuming a direct bandgap (HT AZO: 3.2 eV (ref. 20)).

2.3 Solar cell experiments

The performance of HT and LT AZO was compared in experiment A. The layer stack is displayed in Fig. 1 and the statistics of the key parameters of the investigated devices are summarized in Fig. 4. The thickness of the EELs was varied from 25 over 120 to 220 nm for HT AZO and from 40 over 120 to 240 nm for LT AZO. The V_{OC} of all devices is sufficiently high and comparable. For the j_{SC} we observe some statistical variation without a specific trend. The FF trend is more interesting and relevant to discuss. The FF of the devices with the two thinnest EELs is above 55%, while for the devices with the thickest AZO (>200 nm) layers it is in the 50–55% regime. Analyzing the device with the one diode model and comparing the series and parallel resistance reveals that the series resistance is comparably low for all AZO layers. At a series resistance <1 Ω cm^2, no losses in the FF are expected (Fig. 4e). The shunt resistance is sufficiently high for all configurations (Fig. 4f). The photoshunt resistance, which is the shunt resistance of the illuminated curve, shows a slight trend to lower values for higher AZO film thicknesses (Fig. 4g). The efficiency of LT AZO at 140 °C matches the performance of the HT AZO processed at 260 °C in film conductivity and solar cells.

The simulations in Section 2.1 predict that with the conductivity of LT AZO, a several hundred nanometer EEL should be possible. In experiment B, up to 680 nm thick LT AZO EELs were incorporated into the solar cells to verify the prediction. The illuminated *j–V* characteristics of the devices are displayed in Fig. 5 and the key parameters are listed in Table 2. For the thickest tested film, the R_S still stays low at around 1 Ω cm^2. Therefore, the performance of the devices is comparable in FF (~60%) and V_{OC} (~0.56 to 0.58 V) for all tested thicknesses. The j_{SC} varies around ~1 mA cm^2 which can be due to the morphology of the very thick films and optical effects (see ESI S4†). All that combined the reduction of the PCE for thick films, even up to 680 nm, is only 10% compared to the 100 nm AZO film.

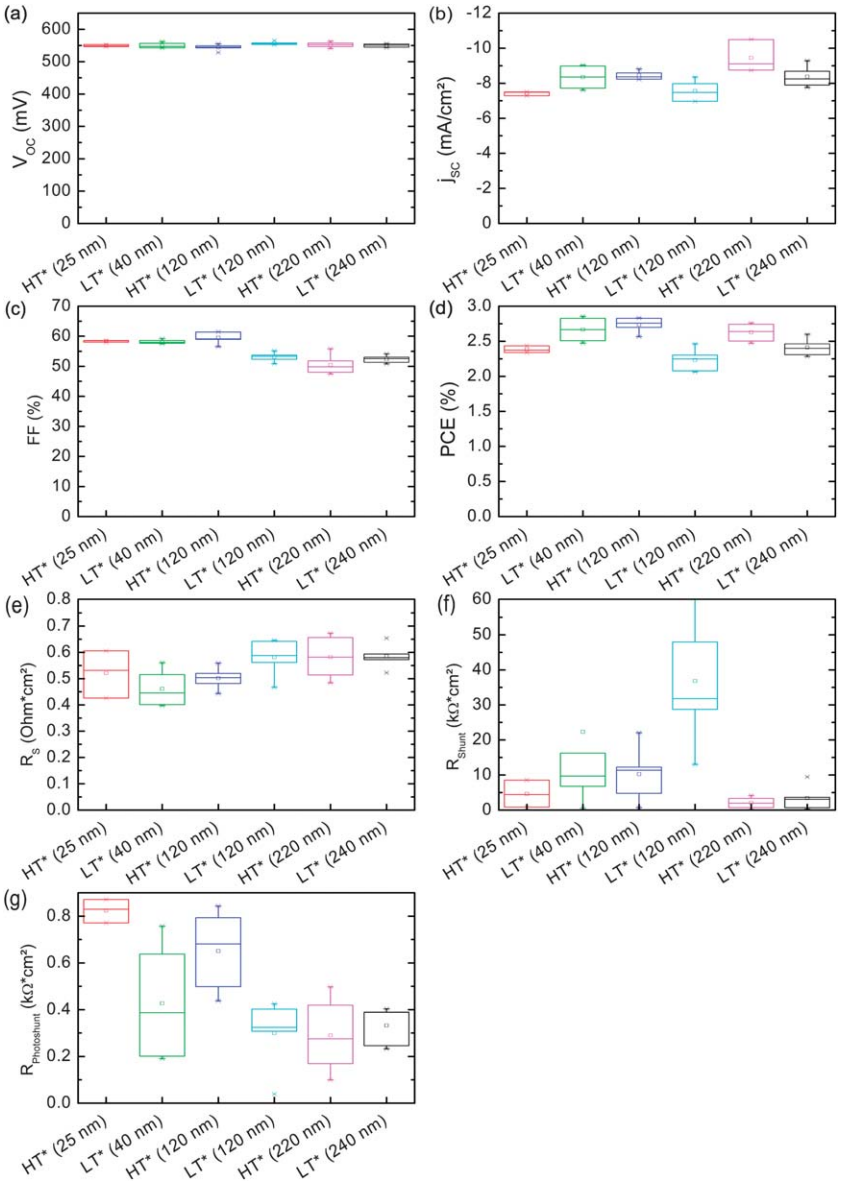

Fig. 4 Key parameters (V_{OC}, FF, j_{SC}, PCE, R_S, R_{Shunt} and $R_{Photoshunt}$) of the investigated devices in experiment A with AZO layers from two different precursors* and annealing conditions as a function of EEL thickness (*HT = high temperature (260 °C) annealed AZO 1 (AlAc, MEA stabilized), LT = low temperature (140 °C) annealed AZO 3 (AlNi, filtered)).

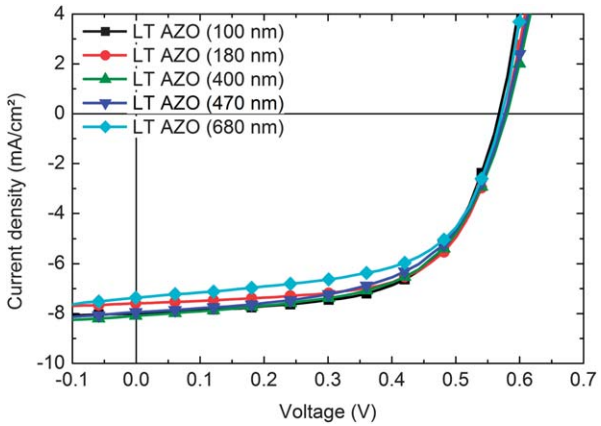

Fig. 5 Illuminated *j–V* characteristics of experiment B with different thicknesses (100–680 nm) of the low temperature (140 °C) processed AZO 3 (LT AZO) EELs.

Table 2 Key parameters of the devices of experiment B with different thicknesses (100–680 nm) of the low temperature (140 °C) processed AZO 3 (LT AZO) EELs

LT AZO	V_{OC} (V)	j_{SC} (mA cm^{-2})	FF (%)	PCE (%)
100 nm	0.57	7.98	61.4	2.79
180 nm	0.58	7.59	63.4	2.79
400 nm	0.57	8.09	58.6	2.70
470 nm	0.58	7.94	58.1	2.68
680 nm	0.57	7.37	60.0	2.52

3 Conclusion

Through a systematic variation of the AZO precursor materials, an improved formulation for highly conductive AZO layers processed at low temperatures was identified. The filtered precursor comprising an aluminum nitrate dopant (AZO 3) shows the best electrical properties ($\sigma = 7 \times 10^{-3}$ S cm^{-1}) at 140 °C (LT AZO). The conductivity of these layers matches the films of the previously investigated formulation AZO 1 at 260 °C (HT AZO) and is above the simulated threshold to overcome the thickness restriction for interface layers ($\sigma = 1 \times 10^{-3}$ S cm^{-1}). As a result, the performance of these two films as EELs in polymer solar cells is also good and comparable. Even when applying the LT AZO EEL with thicknesses of 680 nm, the efficiency and the series resistance of the devices are still comparable to the ones with thin EELs.

4 Experimental section

4.1 Synthesis of Al doped ZnO precursors (routes partly adopted from ref. 27 and 28: doping ratio: 1 at.% Al)

AZO 1 (AlAc, MEA): $Zn(Ac)_2 \cdot 2H_2O$ (2.20 g), $Al(Ac)_2OH$ (0.016 g) and ethanolamine (MEA, 0.16 mL) were mixed in 100 mL of ethanol. The mixture was heated to 80 °C for 2.5 h. As a result, a clear solution was obtained.

AZO 2 (AlAc, filtered): $Zn(Ac)_2 \cdot 2H_2O$ (2.20 g) and $Al(Ac)_2OH$ (0.016 g) were mixed in 100 mL of ethanol. The mixture was heated to 80 °C for 2.5 h and afterwards filtered through a 0.45 micron filter to remove the insoluble material.

AZO 3 (AlNi, filtered): $Zn(Ac)_2 \cdot 2H_2O$ (2.17 g) and $Al(NO_3)_3 \cdot 9H_2O$ (0.038 g) were mixed in 100 mL of ethanol. The mixture was heated to 80 °C for 2.5 h and afterwards filtered through a 0.45 micron filter to remove the insoluble material.

4.2 Solar cell processing

The inverted photovoltaic devices were processed and characterized in ambient atmosphere. Pre-structured ITO coated glass substrates (as obtained from Osram) were subsequently cleaned in acetone and isopropyl alcohol for 10 minutes each. After drying, the substrates were coated with the two different organic precursors for AZO *via* doctor blading. Conversion of the precursors to AZO *via* hydrolysis was achieved by heating the samples to 260 °C or 140 °C for 10 min depending on the configuration. Higher layer thicknesses were achieved *via* subsequent deposition and annealing steps. P3HT purchased from Merck and technical grade PCBM from Solenne were separately dissolved in chlorobenzene at a concentration of 2 wt % and stirred for at least 1 h at 60 °C before being blended in a volume ratio of 1 : 1. The blended solution was stirred for at least another hour at 60 °C before use. The *ca.* 100 nm thick active layer was deposited *via* doctor blading. PEDOT:PSS (Clevios PH) from H.C. Starck was diluted in isopropyl alcohol (1 : 5 volume ratio) before deposition of an approx. 50 nm thick film *via* doctor blading. The whole stack was annealed at 140 °C for 10 min on a hot plate before evaporation of a 100 nm thick Ag layer to form the top electrode. The active area of the investigated devices was 10.4 mm^2. Current density–voltage (*j–V*) characteristics were measured with a source measurement unit from BoTest. Illumination was carried out using an Oriel Sol 1A Solar simulator with AM1.5G spectra at 0.1 W cm^{-2}. A UV-VIS-NIR spectrometer (Perkin – Lambda 950) was used for optical characterization of the thin films.

4.3 Transistor fabrication

The transistor devices were fabricated on a heavily p-doped silicon wafer with 100 nm thermally grown silicon dioxide. The gate electrodes were formed by evaporating 30 nm aluminum through a shadow mask. Then a solution of poly(4-vinylphenol) (PVP) and the cross-linking agent poly(melamine-*co*-formaldehyde) in propylene glycol monomethyl ether acetate was spin-coated at 4000 rpm for 20 s, dried for 1 min at 100 °C and subsequently cross-linked at 200 °C for 6 min. The resulting PVP dielectric layer had a thickness of about 190 nm and a capacitance of 90 nF cm^{-2}. Then the different AZO layers were doctor bladed and annealed before the evaporation of 30 nm thick aluminum layers as top electrodes forming channels with a length of 40 μm and a width of 600 μm.

Acknowledgements

The authors gratefully acknowledge the support of the Cluster of Excellence "Engineering of Advanced Materials" at the University of Erlangen-Nuremberg, which is funded by the German Research Foundation (DFG) within the framework of its "Excellence Initiative" as well as the Solar Factory of the Future within the framework of the Energy Campus Nuremberg (EnCN). This work was funded by a German Research Foundation project grant (DFG; Grant no. BR 4031/1-1 and BR 4031/1-2).

References

1 S. Aramaki, *MRS Conference*, Mitsubishi Chemicals, Boston, Symposium H, Oral Presentation, 2011.
2 http://www.heliatek.com/, November 2012.
3 http://newsroom.ucla.edu/portal/ucla/ucla-engineers-create-tandem-polymer-228468.aspx, November 2012.
4 Y. Liang and L. Yu, A new class of semiconducting polymers for bulk heterojunction solar cells with exceptionally high performance, *Acc. Chem. Res.*, 2010, **43**(9), 1227–1236.
5 T.-Y. Chu, J. Lu, S. Beaupré, Y. Zhang, J.-R. Pouliot, S. Wakim, J. Zhou, M. Leclerc, Z. Li, J. Ding and Y. Tao, Bulk heterojunction solar cells using thieno[3,4-*c*]pyrrole-4,6-dione and dithieno[3,2-*b*:2′,3′-*d*]silole copolymer with a power conversion efficiency of 7.3%, *J. Am. Chem. Soc.*, 2011, **133**(12), 4250–4253.
6 J. Peet, L. Wen, P. Byrne, S. Rodman, K. Forberich, Y. Shao, N. Drolet, R. Gaudiana, G. Dennler and D. Waller, Bulk heterojunction solar cells with thick active layers and high fill factors enabled by a bithiophene-*co*-thiazolothiazole push–pull copolymer, *Appl. Phys. Lett.*, 2011, **98**(4), 043301.
7 E. Voroshazi, B. Verreet, A. Buri, R. Müller, D. D. Nuzzo and P. Heremans, Influence of cathode oxidation *via* the hole extraction layer in polymer:fullerene solar cells, *Org. Electron.*, 2011, **12**(5), 736–744.

8 M. Jørgensen, K. Norrman and F. C. Krebs, Stability/degradation of polymer solar cells, *Sol. Energy Mater. Sol. Cells*, 2008, **92**(7), 686–714.
9 K. Norrman, S. A. Gevorgyan and F. C. Krebs, Water-induced degradation of polymer solar cells studied by $H_2{}^{18}O$ labeling, *ACS Appl. Mater. Interfaces*, 2009, **1**(1), 102–112.
10 T. Stubhan, N. Li, N. A. Luechinger, S. C. Halim, G. J. Matt and C. J. Brabec, High fill factor polymer solar cells comprising a low temperature solution processed WO_3 hole extraction layer, *Adv. Energy Mater.*, 2012, **2**, 1433–1438.
11 T. Stubhan, T. Ameri, M. Salinas, J. Krantz, F. Machui, M. Halik and C. J. Brabec, High shunt resistance in polymer solar cells comprising a MoO_3 hole extraction layer processed from nanoparticle suspension, *Appl. Phys. Lett.*, 2011, **98**, 253308.
12 K. Zilberberg, S. Trost, H. Schmidt and T. Riedl, Solution processed vanadium pentoxide as charge extraction layer for organic solar cells, *Adv. Energy Mater.*, 2011, **1**, 377–381.
13 K. X. Steirer, P. F. Ndione, N. E. Widjonarko, M. T. Lloyd, J. Meyer, E. L. Ratcliff, A. Kahn, N. R. Armstrong, C. J. Curtis, D. S. Ginley, J. J. Berry and D. C. Olson, Enhanced efficiency in plastic solar cells *via* energy matched solution processed NiO_x interlayers, *Adv. Energy Mater.*, 2011, **1**, 813–820.
14 H. Oh, J. Krantz, I. Litzov, T. Stubhan, L. Pinna and C. J. Brabec, Comparison of various sol–gel derived metal oxide layers for inverted organic solar cells, *Sol. Energy Mater. Sol. Cells*, 2011, **95**, 2194–2199.
15 C. Waldauf, M. Morana, P. Denk, P. Schilinsky, K. Coakley, S. A. Choulis and C. J. Brabec, Highly efficient inverted organic photovoltaics using solution based titanium oxide as electron selective contact, *Appl. Phys. Lett.*, 2006, **89**, 233517.
16 Y. Sun, J. H. Seo, C. J. Takacs, J. Seifter and A. J. Heeger, Inverted polymer solar cells integrated with a low-temperature-annealed sol–gel-derived ZnO film as an electron transport layer, *Adv. Mater.*, 2011, **23**, 1679.
17 M. S. White, D. C. Olson, S. E. Shaheen, N. Kopidakis and D. S. Ginley, Inverted bulk-heterojunction organic photovoltaic device using a solution-derived ZnO underlayer, *Appl. Phys. Lett.*, 2006, **89**, 143513.
18 J. Gilot, M. M. Wienk and R. A. J. Janssen, Double and triple junction polymer solar cells processed from solution, *Appl. Phys. Lett.*, 2007, **90**, 143512.
19 F. C. Krebs, All solution roll-to-roll processed polymer solar cells free from indium-tin-oxide and vacuum coating steps, *Org. Electron.*, 2009, **10**, 761–768.
20 T. Stubhan, H. Oh, L. Pinna, J. Krantz, I. Litzov and C. J. Brabec, Inverted organic solar cells using a solution processed aluminum-doped zinc oxide buffer layer, *Org. Electron.*, 2011, **12**, 1539–1543.
21 A. Puetz, T. Stubhan, M. Reinhard, O. Loesch, E. Hammarberg, S. Wolf, C. Feldmann, H. Kalt, A. Colsmann and U. Lemmer, Organic solar cells incorporating buffer layers from indium doped zinc oxide nanoparticles, *Sol. Energy Mater. Sol. Cells*, 2011, **95**, 579–585.
22 E. Schricker, Diplomarbeit, Friedrich-Alexander-University Erlangen-Nuremberg.
23 http://www.pv.unsw.edu.au/info-about/our-school/products-services/pc1d/, June 2012.
24 W. Tress, K. Leo and M. Riede, Influence of hole-transport layers and donor materials on open-circuit voltage and shape of *I–V* curves of organic solar cells, *Adv. Funct. Mater.*, 2011, **21**, 2140–2149.
25 M. Vafaee and M. S. Ghamsari, Preparation and characterization of ZnO nanoparticles by a novel sol–gel route, *Mater. Lett.*, 2007, **61**, 3265–3268.
26 S. H. Yoon, D. Liu, D. Shen, M. Park and D.-J. Kim, Effect of chelating agents on the preferred orientation of ZnO films by sol–gel process, *J. Mater. Sci.*, 2008, **43**, 6177–6181.
27 R. Søndergaard, M. Helgesen, M. Jørgensen and F. C. Krebs, Fabrication of polymer solar cells using aqueous processing for all layers including the metal back electrode, *Adv. Energy Mater.*, 2011, **1**, 68–71.
28 M. J. Alam and D. C. Cameron, Preparation and properties of transparent conductive aluminum-doped zinc oxide thin films by sol–gel process, *J. Vac. Sci. Technol.*, 2001, 1642–1646.